DOI: 10.24874/ti.1510.07.23.09

Tribology in Industry

www.tribology.rs

RESEARCH

Influence of Variable Depth Surface Texture on the Performance Behaviours of Sector Shape Pad Thrust Bearing

Shipra Aggarwal[a]

[a]*Mechanical & Automation Engineering Department, Indira Gandhi Delhi Technical University for Women, Kashmere Gate, Delhi 110006, India.*

Keywords:

Pocket
Surface texture
Groove
Hydrodynamic lubrication
Thrust pad bearing
Coefficient of friction

* Corresponding author:

Shipra Aggarwal
E-mail: shipraagg@gmail.com

Received: 3 July 2023
Revised: 15 August 2023
Accepted: 24 September 2023

A B S T R A C T

Performance behaviours of oil-lubricated sector shape pad thrust bearings incorporating the variable depth's pockets/textures have been presented. The variable depth texture comprises of combination of grooves and pockets. Fixed depth pocket, variable depth pocket (depth of the pocket reducing towards the exit) and combination of fixed and variable depth pocket with the fixed and variable depth grooves have been considered in the present investigation. With the aim to improve the performance parameters of fixed pad thrust bearing, the effect of texture parameters such as pocket/groove depth, the circumferential extent of texture and different combinations of variable depth's pocket and grooves have been investigated. Substantial improvement in the performance parameters (minimum film thickness and coefficient of friction) has been achieved in the presence of proposed textures having variable depths of micro-geometries.

1. INTRODUCTION

Fluid film thrust pad bearings are commonly employed to support and guide the axial/thrust loads in hydraulic and steam turbines, air compressors, automobiles and high-power rated helical gearboxes [1-5]. Due to the widespread utilization of thrust pad bearings, numerous efforts are being made by researchers to study and improve their tribo-dynamic behaviours [5-6]. Owing to the growing thrust on energy conservation and new demands of operational conditions, researchers have attempted from time to time to enhance the performance behaviours of thrust pad bearings using different techniques. Researchers have employed various surface topographies such as surface textures [1-6] and surface profiles [7-10] to improve the performances. It is reported that film shape [11] and surface topographies/textures [12-14] play a vital role in the effective development of hydrodynamic pressure and accordingly lead to improvement in the performance parameters.

The roles of surface textures in improving the performance behaviours (reducing the friction

and increasing minimum film thickness) of hydrodynamic bearings and other tribo-contacts are being widely explored and practised [12-18]. Investigations have been done by researchers [16] to find the optimal geometrical shapes and depths of surface textures with a view to achieving lower friction, higher load-carrying capacity, and lesser rise in temperature. It is also revealed that texture depth has a strong influence on the bearing performance [17-19]. In this direction, numerous efforts have been made by researchers [17-19] to find the optimum texture depth employing constant depth texture. It is reported that optimum texture depth is impacted by operating conditions [19] and convergence ratio [17].

The micro-geometries of the textures on the interacting surfaces lead to the creation of micro-wedges, which serve as micro hydrodynamic bearings that support higher loads. Micro-dimples and micro-pockets act as numerous micro-pools of lubricant under severe operating conditions and during starting/stopping and can also trap the wear particles and contaminants which improve the reliability and life of the lubricated contacts [20-22]. However, due to the formation of the diverging zone in the presence of micro-geometries in textures, rupture of the fluid film may take place, and hence cavitation effect must be considered in the model which makes it a little involved task [5,23].

It is noticed that researchers have employed different micro-geometries such as pockets, grooves, pits and dimples in textures on the pads' surface. It is revealed that open-pocketed pad bearing yields higher load-carrying capacity in comparison to other bearings [24]. It is reported that a pad having a rectangular-shaped micro-pocket enhanced the minimum film thickness up to 232% with reference to plain thrust pad bearing [25]. Some novel pockets along with bionic textures have been proposed by researchers [25-27], which comprised rectangular and trapezoidal shape pockets. These micro-pockets further improved the performance behaviours in comparison to rectangular-shaped pockets. Grooves oriented between 30 degrees to 60 degrees reduced the friction by up to 44% with respect to the untextured case [28].

Recently, micro-grooves have also been used [19, 28] to improve the performance behaviours of lubricated interfaces. Higher load-carrying capacity (97%) and lower friction coefficient (51%) have been reported [4]. A comparative study of pocketed and circumferential grooved pads yielded an improvement in minimum film thickness by 24% for the pocketed bearing and by 20% in the presence of circumferential micro-grooves [19].

On the basis of literature review, it is found that the performance behaviours of fluid film bearings are greatly influenced by the depth of micro-geometries in the textures. The authors [24, 29] have explored the effects of variation of depths (by keeping depth constant for each case of run) of micro-geometries present in texture on the performance parameters of the bearing. However, the present author could not notice any exploratory research employing variable depth pockets/grooves in textures. Therefore, the objective of exploration was set to numerically investigate the influence of variable depth pocket/groove of texture on the performance behaviours of a fixed thrust pad bearing. In a variable depth of pocket, the depth of the pocket is changing along its length in the circumferential direction. Therefore, the investigations have been carried out by employing constant depth pocket, variable depth pocket and a combination of variable depth grooves and variable depth pocket on the pad surface.

2. MATHEMATICAL MODELLING

A fixed thrust pad bearing of sector shape is considered in the proposed mathematical model. The surface of the pad is textured comprising of pocket and a combination of pocket and circumferential grooves. Schematic views of the textured pads have been shown in Fig. 1.

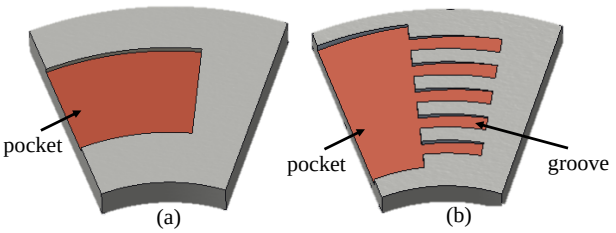

Fig. 1. Schematic views of textured pads; (a) pocketed, (b) combination of pocket and grooves.

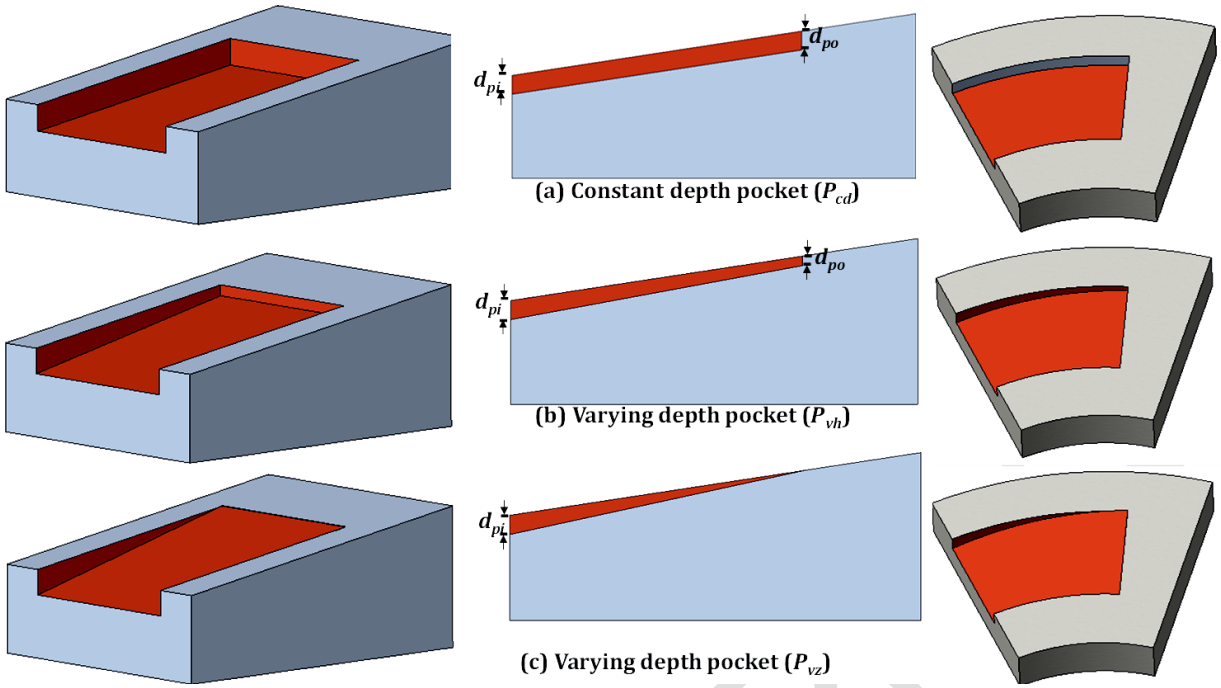

Fig. 2. CAD views of pocketed pads; (a) with constant depth of pocket, (b) with varying depth of pocket (case-1), (c) with varying depth of pocket (case-2).

In this analysis, constant depth pocket and variable depth pocket [in which depth of the pocket is reducing along its length; depth varying to half of the initial depth (case-1), and depth varying to zero (case-2)] have been considered. The CAD illustrations of constant and variable depths pockets are presented in Fig. 2. In the present analysis, an open rectangular-shaped pocket has been considered. Figure 3 shows the schematic view of the placement of pocket and grooves on the pad for the development of film thickness expressions.

Expression for film thickness for the plain pad is as follows [30]:

$$\bar{h}_{plain} = 1 + \left(\frac{h_1}{h_2} - 1\right)\left(1 - \frac{\theta}{\theta_0}\right) \tag{1}$$

Modification in the expression of film thickness takes place due to the presence of pocket/groove on the pad surface. Modified film thickness is modelled utilizing the following expressions [4,5]:

$$\bar{h} = \bar{h}_{plain} + \bar{h}_p + \bar{h}_g \tag{2}$$

For constant depth pocket-

$$\bar{h}_p = \begin{cases} d_{pi}/h_2, & \theta \le \theta_p \\ 0, & \text{else} \end{cases} \tag{3}$$

For variable depth pocket (P_{vz}, P_{vh}):

$$\bar{h}_p = \begin{cases} \left(\frac{d_{pi}}{h_2}\right) - \left(\frac{d_{pi}-d_{po}}{h_2}\right) * \frac{ii}{N_p}, \\ ii = 1,2,\ldots,N_p \;\; \theta \le \theta_p \\ 0, \;\; \text{else} \end{cases} \tag{4}$$

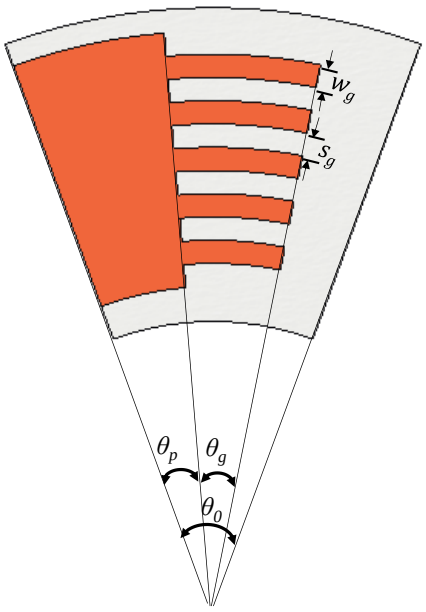

Fig. 3. Schematic view of the placement of pocket and grooves on the pad for the development of film thickness expressions.

For constant depth groove:

$$\bar{h}_g = \begin{cases} \left(\frac{d_{gi}}{h_2}\right) \\ \text{if } \left[(2jj+1)w_g < r < (2jj+2)w_g\right], \\ jj = 1,2,\dots,N_g \;\; \theta \le \theta_p \\ 0, \qquad\qquad \text{else} \end{cases} \quad (5)$$

For variable depth groove:

$$\bar{h}_g = \begin{cases} \left(\frac{d_{gi}}{h_2}\right) - \left(\frac{d_{gi}-d_{go}}{h_2}\right) * \frac{ii}{N_g}, \\ ii = 1,2,\dots,N_g, \\ \text{if } \left[(2jj+1)w_g < r < (2jj+2)w_g\right], \\ jj = 1,2,\dots,N_g \; \theta \le \theta_p \\ 0, \;\text{else} \end{cases} \quad (6)$$

Assuming non-inertial laminar, viscous, and steady-state flow of lubricant, the Reynolds equation adopted in present model incorporating the Elrod's mass-conservative algorithm is [4,31]:

$$\frac{1}{\bar{r}^2}\frac{\partial}{\partial\bar{\theta}}\left(g\frac{\bar{h}^3}{\eta}\frac{\partial\phi}{\partial\bar{\theta}}\right)+\frac{1}{\bar{r}}\frac{\partial}{\partial\bar{r}}\left(g\frac{\bar{r}\bar{h}^3}{\eta}\frac{\partial\phi}{\partial\bar{r}}\right)=\lambda\frac{\partial}{\partial\bar{\theta}}(\bar{h}\phi) \quad (7)$$

where

$$\phi=\frac{\rho}{\rho_c},\ \beta=\rho\frac{\partial p}{\partial\rho}\ ,\ \lambda=\frac{6\eta\omega R_m^2}{h_2^2\beta}\ ,$$

g=1 when $\phi \ge 1$; g =0 when ϕ <1

$$\bar{h}=\frac{h}{h_2},\ \bar{r}=r/R_m\ ,\ \bar{\theta}=\theta,\ R_m=(R_1+R_2)/2$$

Equation (7) is solved for 'ϕ' at different nodes in the domain by initializing it with a value of 1.000006 and assuming full film at the inlet edge. Thereafter, values of pressure at different nodes are computed employing the following relation [21]:

$$p = p_c + g\beta \ln\phi \quad (8)$$

The computed pressure values at different nodes is then integrated to calculate the value of load carrying capacity using the relation as mentioned below [4, 30]:

$$\overline{W} = \int_{\bar{R}_1}^{\bar{R}_2}\int_0^{\theta_0}\overline{pr}\,d\bar{r}\,d\bar{\theta} \quad (9)$$

where $\bar{p} = p\square_2^2/(\eta\omega R_m^2)$

Coefficient of friction is computed employing the following relation [4,30]:

$$\mu = \frac{\bar{F}}{\bar{W}}\left(\frac{h_2}{R_m}\right) \quad (10)$$

where $\overline{F} = \int_{\bar{R}_1}^{\bar{R}_2}\int_0^{\theta_0}\left[\frac{\overline{\eta}}{\bar{h}}\frac{\partial v_\theta}{\partial\bar{z}}\right]\bar{r}d\bar{r}d\bar{\theta}$

3. COMPUTATIONAL PROCEDURE

The finite difference method is used to discretise the eqn. (7), thereafter, Gauss Siedel iterative procedure is used for solving the nodes linked algebraic equations [4, 9]. The results have been computed employing 301 (N_θ) x 301 (N_r) grids, which has been found based on the grid independence test. The following convergence criterion has been adopted in the computation:

$$\frac{\sum_{i=1}^{N_\theta}\sum_{j=1}^{N_r}\left|\varphi(i,j)_{new}-\varphi(i,j)_{old}\right|}{\sum_{i=1}^{N_\theta}\sum_{j=1}^{N_r}\left|\varphi(i,j)_{new}\right|} \le 10^{-8} \quad (11)$$

During the numerical solution, the load balancing has been done by adjusting the value of minimum film thickness (h_2).

4. VALIDATION OF MODEL

To have confidence in the proposed mathematical model, the computed results have been validated with the published works of researchers [31, 33]. A parabolic slider has been adopted by the authors [31] in their work having converging and diverging geometries. Thus, this case has been adopted to validate the results achieved from solution of mass conservation aspects covering Reynolds equation. Good matching between the calculated pressure values and the values reported in the published work [31] can be seen in Fig.4(a). Moreover, present model-based result has been compared with a textured pad case [33] result in Fig. 4(b). In this case too, a good matching/correlation between both the results can be observed, hence, the proposed model has been considered validated.

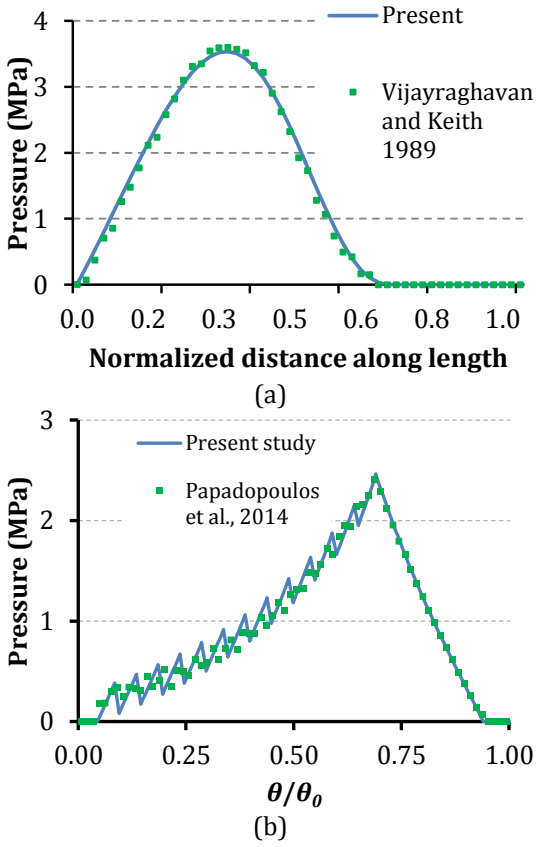

Fig. 4. Validation of the proposed model with prior published work (a) Pressure distribution with Vijayraghavan and Keith, 1989 [β=6.9x10^7 Pa, η_0=0.039 Pa-s, L=0.0762 m, U=4.57 m/s] (b) Pressure profile with Papadopoulus et al., 2014 [η_0=0.0416 Pa-s, N=5000 rpm, θ_0=45^0, h_2=30 µm, h_d=20 µm, R_1=0.025 m, R_2=0.045 m].

5. RESULTS AND DISCUSSION

Numerical results have been presented employing the input data (R_1=0.025 m, R_2= 0.052 m, s_h=16.2 µm, η_0=0.139 Pa-s, θ_0=40^0, N=3000 rpm, radial extent of pocket=80%). The variations (with reference to the plain pad) in the minimum film thickness (h_2) and coefficient of friction (μ) [keeping shoulder height and unit load constant] with the depth of the pocket at the inlet have been presented in Figs. 5 and 6 at unit loads of 2 MPa and 5 MPa, respectively, for three cases as mentioned below:

- constant depth pocket (p_{cd}),
- variable depth pocket (p_{vh}): depth reduced to half of inlet depth along the length of the pocket (d_{po}=0.5d_{pi})
- variable depth pocket (p_{vz}): pocket depth reduced to zero (d_{po}=0).

It can be noticed in Fig. 5(a) that the presence of pocket yields an increase in the minimum film thickness (h_2). With increase in depth of pocket, film thickness (h_2) increases, attains a maximum value and decreases thereafter. Up to 32% increase in minimum film thickness has been found with variable depth pocket (p_{vz}) having 80 µm depth of the pocket at the entry. However, with pocket's constant depth of 35 µm and variable depth (p_{vh}) of 50 µm, 23% and 30% enhancement in minimum film thickness has been achieved, respectively.

Figure 5(b) shows the reduction in friction coefficient with different pocketed pads in comparison to conventional plain pad. Around 30% decrease in the value of μ has been found with constant pocket's depth of 50 µm. However, with variable depth pocketed pads (p_{vh} and p_{vz}), marginally better results have been achieved as compared to previous case.

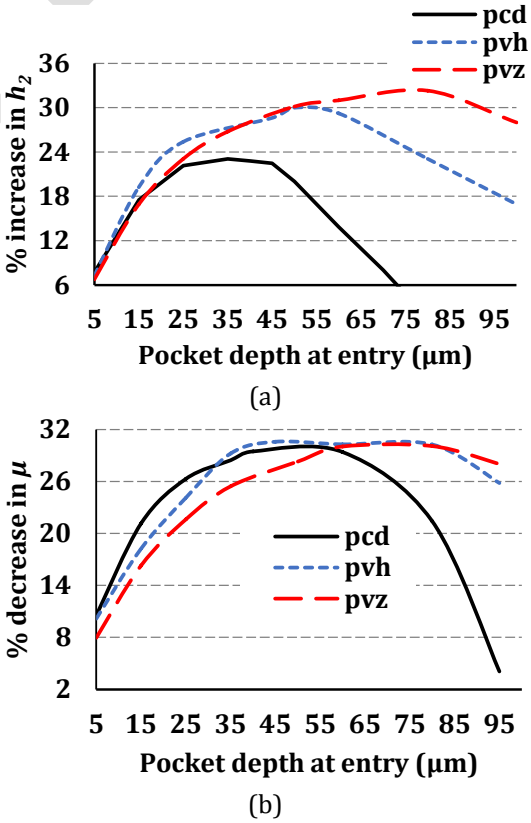

Fig. 5. Percentage changes in performance parameters; (a) enhancement in h_2, (b) decrease in μ [unit load =2 MPa, θ_p/θ_o=0.7].

However, when the unit load is increased to 5 MPa, the maximum increase in h_2 reduces and attains a maximum value of 21% for a variable depth pocket (p_{vh}) as can be viewed in Figure

6(a) for a 35 μm deep pocket. Maximum enhancement of around 18% is achieved with a constant depth pocket (25 μm deep) and around 20.5% increase in h_2 is noticed for a variable depth pocket (p_{vz} at 50 μm deep). Reduction in the values of film thickness (h_2) owing to the enhancement in the load is consistent as per the findings reported in reference [5]. It is pertinent to mention here that the magnitude and location of the highest rise in the film thickness (h_2) vary with the pockets' depth and type of pocket depending on the applied load.

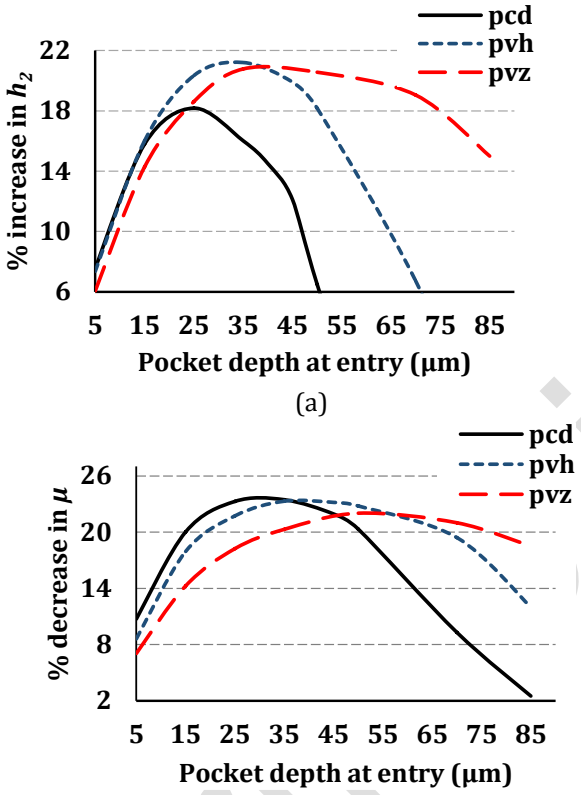

Fig. 6. Variation of performance behaviours (a) enhancement in film thickness (b) decrease in friction coefficient for different pocketed pads with reference to plain conventional pad [unit load =5 MPa, θ_p/θ_o=0.7].

Moreover, Fig. 6(b) demonstrates the reduction in the friction coefficient (μ) with a variation of the pocket's depth. A maximum reduction in the friction coefficient is seen in the range of 21-23% for all the pocketed pads considered in the analysis. However, the depth at which maximum reduction in μ is achieved for different pocketed pads agrees with the depth of pockets at which maximum increase in h_2 is observed (refer Fig. 6(a)).

In order to understand the mechanism leading to the enhancement in film thickness (h_2) and reduction in μ, six sections have been considered (1-1', 2-2', 3-3', 4-4', 5-5' and 6-6') along the circumferential direction of pad as shown in Fig. 7(a). The dimensionless flow rates have been calculated at different sections for different pocketed and plain pads as shown in Fig. 7(b).

It is noticed that a steep decrease in flow rate has happened around section planes (2–2' and 5–5') for constant depth and variable depth pocketed pad (p_{vh}) and along (2–2' and 6–6') for variable depth pocketed pad (p_{vz}) which results in higher pressure enhancement as compared to conventional plain pad.

The steep reduction in flow rate occurs due to the presence of constriction towards the exit side on the pocket. This phenomenon causes increase in pressure in oil film as can be seen in Figs. 7(c) and 7(d). Thus the synergistic effect of pressure gradient and film thickness variation produces reduction in friction force. Relative low value of friction force has been found with variable depth pocket as compared to plain pad case. The low value of friction force when divided by the same magnitude of load results in a lower friction coefficient in the case of pocketed pads in comparison to plain pad.

Therefore, it is worth noting here that superior performance is achieved with pocketed pads due to reduced flow, which results in an enhancement in the lubricant film pressure and lubricant film thickness. The pressure distribution in 3D for a variable pocketed pad is illustrated in Figure 7(c). Moreover, the 2D pressure curves at the mean radius attained with different pocketed pads along with the plain pad are illustrated in Fig.

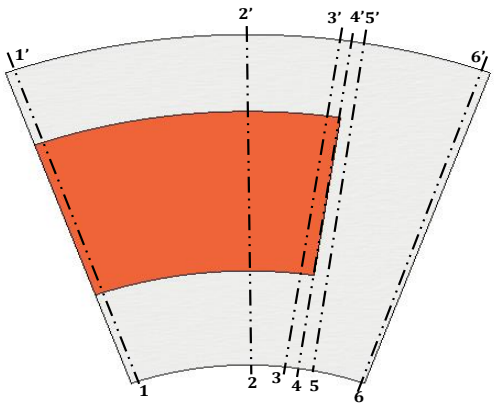

(a)

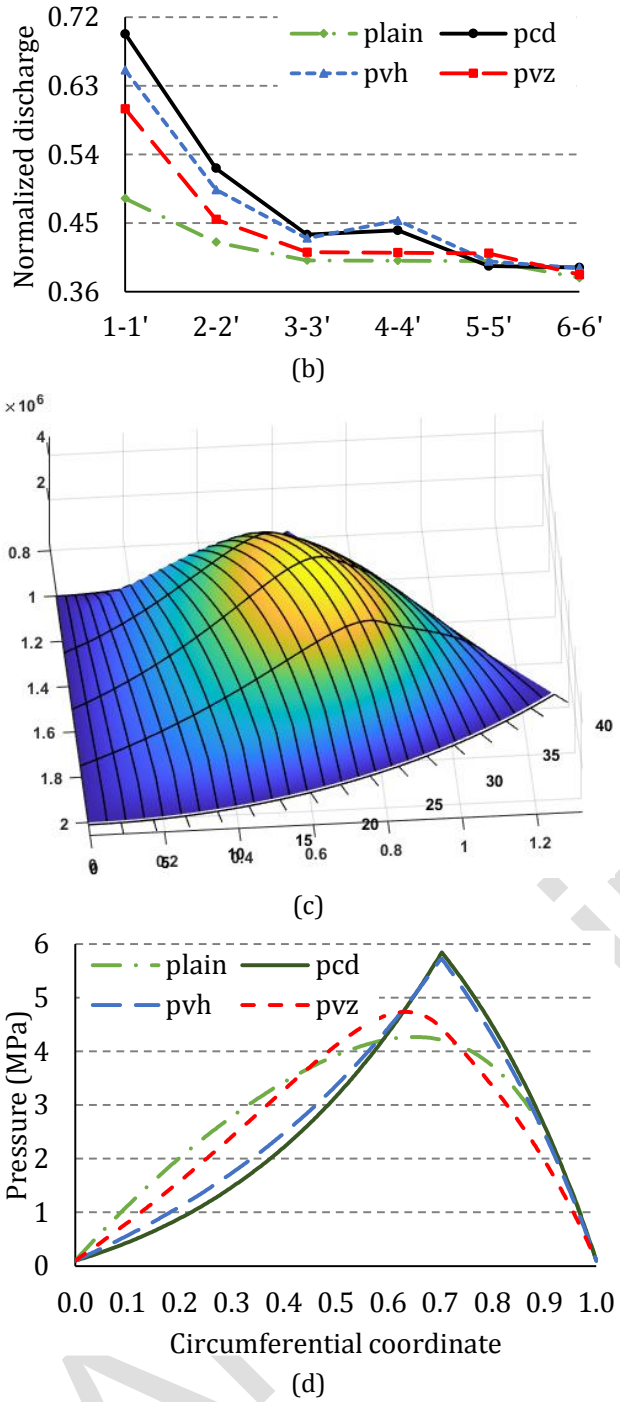

Fig. 7. Performance parameters' variation; (a) sectional position at which discharge is computed (b) normalized discharge at different sections (c) 3-D pressure distribution of variable depth pocketed pad (d) pressure distribution in the circumferential direction at mid-section of the plain pad and pad having pockets of constant and variable depths [Unit load=2 MPa, θ_p/θ_o=0.7, d_{pi}= 40 μm].

7(d). It can be noticed that a larger magnitude of peak pressure at mid-plane along the circumferential direction are obtained with pocketed pads. Similar type of findings is also reported in [5, 34].

The rise in the film thickness (h_2) and decrease in friction coefficient (μ) with non-dimensional circumferential extent (θ_p/θ_0) of the pocket for different pocketed pads in contrast to the conventional plain pad is illustrated in Fig. 8 and Fig. 9. The unit load applied is 2 MPa and 5 MPa respectively. It is observed in Fig. 8(a) and 8(b) that the maximum rise in h_2 and substantial reduction in μ is achieved at 70% circumferential extent of the pocket for constant depth and variable depth pockets considered. The maximum increase of 30% in h_2 is achieved with a variable depth pocket (depth reducing to zero) at 70% circumferential extent. The decrease in μ is the same for the constant depth pocket and variable depth pocket (depth reducing to half), and the maximum reduction in friction coefficient is around 30% for both cases which can be observed in Fig. 8(b). The decrease in μ for the variable depth pocket (depth reducing to zero) is slightly less reaching a value of around 28% at 70% circumferential extent of the pad.

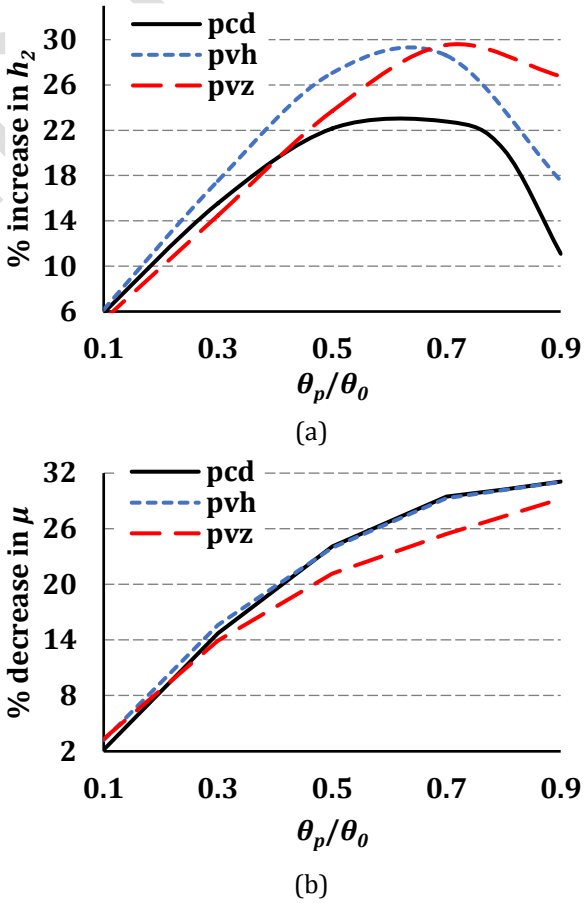

Fig. 8. Variation of performance behaviours (a) increase in film thickness (b) decrease in μ for different pocketed pads with reference to plain conventional pad [unit load =2 MPa, d_{pi}=40 μm].

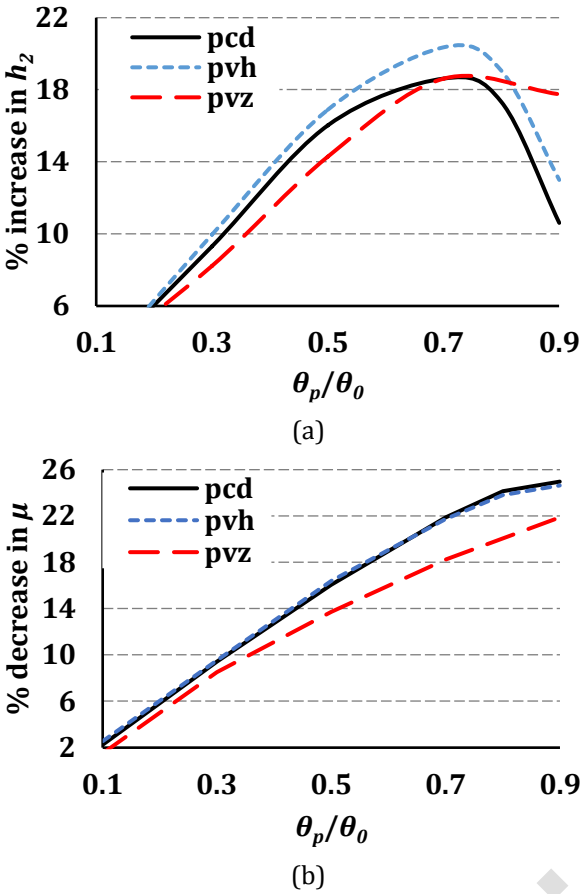

Fig. 9. Variation of performance behaviours (a) enhancement in h_2 (b) decrease in μ for different pocketed pads in comparison to plain conventional pad [unit load =5 MPa, d_{pi}=25 μm].

For 5 MPa unit load, the maximum increase in h_2 is 20% for the variable depth pocket (p_{vh}) and 18% for both the constant depth pocket (p_{cd}) and variable depth pocket (p_{vz}) at 70% circumferential extent of pocket as seen in Fig. 9(a). Moreover, the reduction in μ is 22% for constant depth pocket and variable depth pocket (depth reducing to half) at 70% circumferential extent which can be viewed from Fig. 9(b). Around 18% lesser coefficient of friction is achieved for variable depth pocket (p_{vz}) with reference to plain pad. Therefore, the presence of a pocket up to 70% length of the pad proves advantageous with regard to enhancement of h_2 and reduction of μ. Similar findings have been reported in [34].

In order to explore the benefits of a combination of pocket and circumferential grooves on the performance parameters, numerical simulations have been carried out. A combination of pocket (constant depth, varying depth) and grooves (constant depth, varying depth) have been taken, and the results are presented in Fig. 10. The pocket is spreading up to 50% length of the pad (θ_p/θ_o=0.5), and the grooves are spreading beyond 50% and up to 70% length of the pad($0.5<\theta_g/\theta_o<0.7$). The schematic illustration of the combination of pocketed and grooved pad is shown in Fig. 1(b).

From Fig 10(a) and 10(b), it can be seen that a combination of pocket and grooves results in the enhancement of minimum film thickness and reduction in μ. It can be noticed in Fig. 10(a), a maximum of 29% increase in h_2 is noticed with a combination of varying depth pocket (p_{vh}) which is spreading up to 50% of length and grooves (constant depth, depth varying to half and depth varying to zero) which is spreading beyond 50% and up to 70% of length). The rise in film thickness achieved with constant depth pocket and grooves is in the range of 27-28%. However, less increase (21-23%) in the value of h_2 is obtained with variable depth pocket (p_{vz}) and grooves.

Figure 10(b) shows the reduction in μ for a combination of pocketed and grooved pads in comparison to conventional plain pad. Nearly 27-28% decrease in μ is achieved with a constant depth pocket and variable depth pocket (p_{vh}) as can be seen in Fig. 10(b). However, around 21-23% decrease in μ is observed with a combination of variable depth pocket (p_{vz}) along with grooves.

It is understood that the reason for the relatively low increase in the value of h_2 and μ is due to the diverging region formed at the interface of pocket and grooves in case of variable depth pocket (p_{vz}) and grooves as can be seen in Fig. 11(a). The pressure distribution achieved in Figs. 11(b) and 11(c) reveals the pressure drop at the interface, which also indicates a relatively low restriction of flowing oil.

For unit load 5 MPa, a similar trend of results can be observed in Fig. 12(a) and 12(b) for an increase in h_2 and a decrease in μ for a combination of pocket and grooves. However, the magnitude of the maximum increase in h_2 is limited to 20%, and the maximum reduction in μ is 21%. Therefore, it can be concluded that a combination of pocket (constant depth) and circumferential grooves yield a higher film thickness (h_2) and a lesser friction coefficient (μ) compared to plain pad.

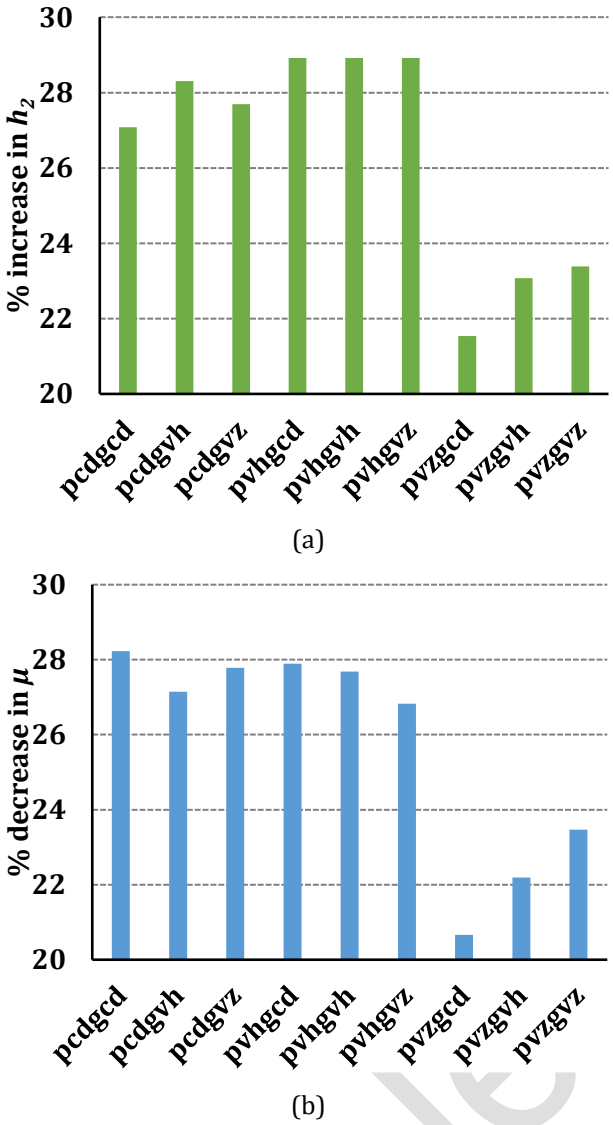

Fig. 10. Variation of performance behaviours (a) enhancement in film thickness (b) reduction in μ for different combinations of pocketed and grooved pads in comparison to plain conventional pad [unit load =2 MPa].

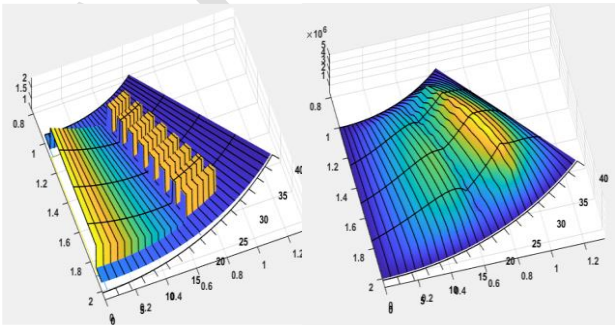

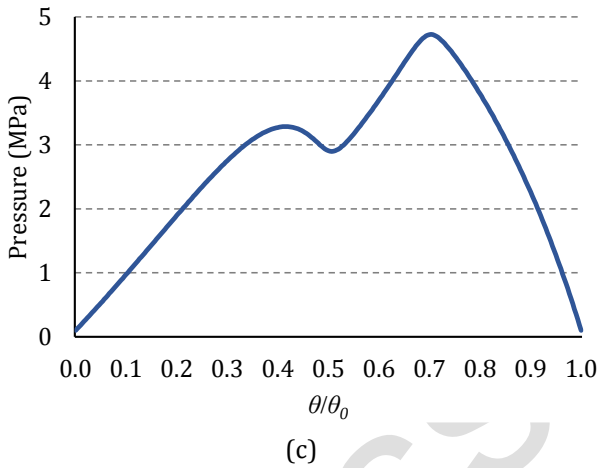

Fig. 11. Variation of (a) 3D film thickness profile; (b) 3-D pressure distribution; (c) Pressure variation in circumferential direction at mid-plane for variable depth pocket (p_{vz}) and constant depth groove (g_{cd}).

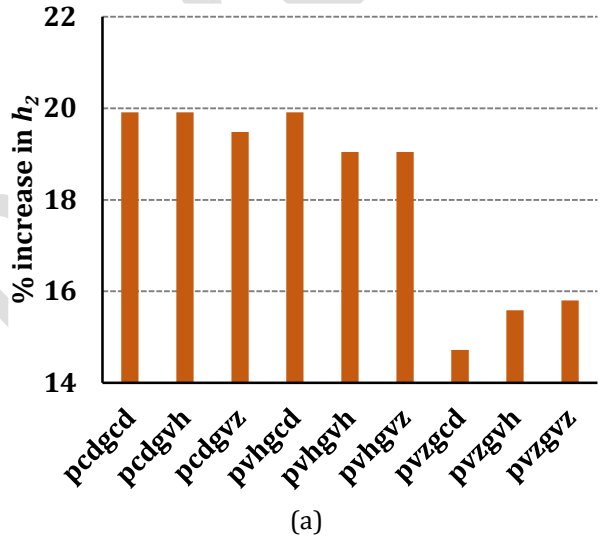

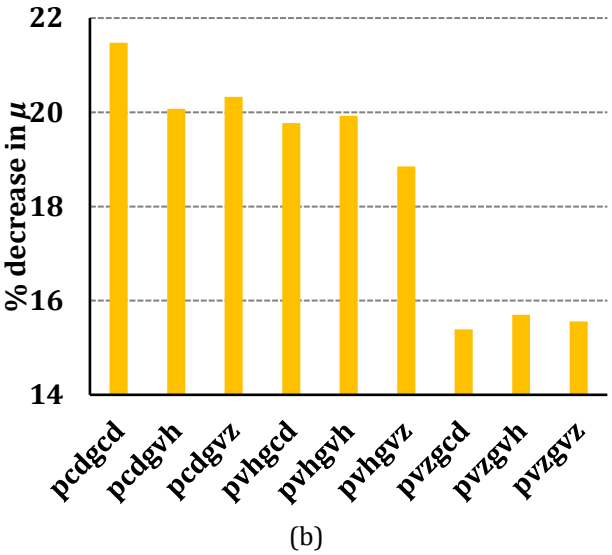

Fig. 12. Variation of performance behaviours (a) enhancement in film thickness (b) reduction in μ for different combinations of pocketed and grooved pads as compared to plain conventional pad [unit load =5 MPa].

6. CONCLUSION

Based on the investigations reported in this work, the following conclusions have been drawn:

1. In the presence of variable depth pocket (depth reducing to half along the length of pocket and depth reducing to zero along the length of pocket) on the fixed pad, significant increase in the minimum film thickness have been found as compared to both the constant depth pocket pad and plain pad.
2. Variable depth pocket (depth reducing to zero along the length) spreading over 70% length of the pad yields the best results i.e. 32% enhancement in minimum film thickness and 30% reduction in friction coefficient with reference to plain pad. It also yielded 7% increase in minimum film thickness in comparison to constant depth pocket.
3. The synergistic presence of the pocket (at the entry) and groove (at the end of pocket) on the pad substantially improved the performance behaviours of thrust pad bearing. Up to 29% increase in minimum film thickness and 28% reduction in coefficient of friction have been found in comparison to plain pad.

REFERENCES

[1] D.J. Ramos, G.B. Daniel, *Microgroove optimization to improve hydrodynamic bearing performance,* Tribology International, vol. 174, pp. 107667, 2022, doi: 10.1016/j.triboint.2022.107667

[2] D.G. Fouflias, A.G. Charitopoulos, C.I. Papadopoulos, L. Kaiktsis, *Thermohydrodynamic analysis and tribological optimization of a curved pocket thrust bearing,* Tribology International, vol. 110, pp. 291-306, 2017. doi:10.1016/j.triboint.2017.02.012

[3] D. Sirohi, S. Aggarwal, *Numerical and Experimental Studies on Performance Enhancement of Thrust Pad Bearing Employing Surface Texture: A Review*, Tribology in Industry, vol. 45, pp. 542-560, 2023, doi: 10.24874/ti.1463.03.23.06

[4] S. Aggarwal, R.K. Pandey, *Frictional and load-carrying behaviours of micro-textured sector shape pad thrust bearing incorporating the cavitation and thermal effects,* Lubrication Science, vol. 29, pp. 255-277, 2017, doi: 10.1002/ls.1367

[5] J.C. Atwal, R.K. Pandey, *Performance analysis of thrust pad bearing using micro-rectangular pocket and bionic texture,* Proceedings of the Institution of Mechanical Engineers, Part J: Journal of Engineering Tribology, vol. 235, iss. 6, pp. 1232-1250, 2021, doi: 10.1177/1350650120940076

[6] G. Shi, X. Yu, H. Meng, F. Zhao, J. Wang, J. Jiao, H. Jiang, *Effect of surface modification on friction characteristics of sliding bearings: A review,* Tribology International, vol. 177, pp. 107937, 2021, doi: 10.1016/j.triboint.2022.107937

[7] A.P. Singh, *An overall optimum design of a sector shaped thrust bearing with continuous circumferential surface profiles,* Wear, vol. 117, pp. 49-77, 1987, doi: 10.1016/0043-1648(87)90244-4

[8] R.K. Sharma, R.K. Pandey, *Experimental studies of pressure distributions in finite slider bearing with single continuous surface profiles on the pads,* Tribol International, vol. 42, pp. 1040-1045, 2009, doi: 10.1016/j.triboint.2009.02.010

[9] S. Aggarwal, *Influence of various single continuous segmental surface profiles for improving the performance parameters of sector shape pad thrust bearing*, Jurnal Tribologi, vol. 37, pp.42-57, 2023.

[10] R.K. Sharma, R.K. Pandey, *Influence of surface profile on slider bearing performance,* International Journal of Surface Science and Engineering, vol. 2, pp. 265–280, 2008, doi: 10.1504/IJSURFSE.2008.020498

[11] Z. Liming, L. Yongyao, W. Zhengwei, L. Xin, X. Yexiang, *A review on the large tilting pad thrust bearings in the hydropower units*, Renewable and Sustainable Energy Reviews, vol. 69, pp. 1182-1198, 2017, doi: 10.1016/j.rser.2016.09.140

[12] D. Gropper, L. Wang, T.J. Harvey, *Hydrodynamic lubrication of textured surfaces: a review of modelling techniques and key findings*, Tribology International, vol. 94, pp. 509-529, 2016, doi: 10.1016/j.triboint.2015.10.009

[13] A. Rosenkranz, H.L. Costa, M.Z. Baykara, A. Martini, *Synergistic effects of surface texturing and solid lubricants to tailor friction and wear-A Review*, Tribology International, vol. 155, pp. 106792, 2021, doi: 10.1016/j.triboint.2020.106792

[14] Z. Wang, R. Ye, J. Xiang, *The performance of textured surfaces in friction reducing: A Review*, Tribology International, vol. 177, pp. 108010, 2023, doi: 10.1016/j.triboint.2022.108010

[15] A. Rosenkranz, H.L. Costa, F. Profito, C. Gachot, S. Medina, D. Dini, *Influence of surface texturing on hydrodynamic friction in plane converging*

bearings-An experimental and numerical approach, Tribology International, vol. 134, pp. 190-204, 2019, doi: 10.1016/j.triboint.2019.01.042

[16] T. Zhirong, M. Xiangkai, M. Yi, P. Xudong, *Shape optimization of hydrodynamic textured surfaces for enhancing load-carrying capacity based on level set method,* Tribology International, vol. 162, pp. 107136, 2021, doi: 10.1016/j.triboint.2021.107136

[17] C.I. Papadopoulos, E.E. Efstathiou, P.G. Nikolakopoulos, L. Kaiktsis, *Geometry optimization of textured three-dimensional micro-thrust bearings,* vol. 133, pp. 041702, 2011, doi: 10.1115/1.4004990

[18] D. Gropper, T.J. Harvey, L. Wang, *Numerical analysis and optimization of surface textures for a tilting pad thrust bearing,* Tribology International, vol. 124, pp. 134-144, 2018, doi: 10.1016/j.triboint.2018.03.034

[19] V. Zouzoulas, C.I. Papadopoulos, *3-D thermohydrodynamic analysis of textured, grooved, pocketed and hydrophobic pivoted-pad thrust bearings,* Tribology International, vol. 110, pp. 426-440, 2017, doi: 10.1016/j.triboint.2016.10.001

[20] Z. Xie, J. Jiao, K. Yang, H. Zhang, *A state-of-art review on the water-lubricated bearing,* Tribology International, vol. 1180, pp. 108276, 2023, doi: 10.1016/j.triboint.2023.108276

[21] Y. Henry, J. Bouyer, M. Fillon, *Experimental analysis of the hydrodynamic effect during start-up of fixed geometry thrust bearings,* Tribology International, vol. 120, pp. 299-308, 2018. doi: 10.1016/j.triboint.2017.12.021

[22] R. Rahmani, H. Rahnejat, *Enhanced performance of optimised partially textured load bearing surfaces,* Tribology International, vol. 117, pp. 272-282, 2018, doi: 10.1016/j.triboint.2017.09.011

[23] S. Aggarwal, R.K. Pandey, Performance investigation of micro-pocketed textured pad thrust bearing. Industrial Lubrication and Tribology, vol. 70, pp. 1388–1395, 2018, doi: 10.1108/ILT-10-2017-0302

[24] D.G. Fouflias, A.G. Charitopoulos, C.I. Papadopoulos, L. Kaiktsis, M. Fillon, *Performance comparison between textured, pocket, and tapered-land sector-pad thrust bearings using computational fluid dynamics thermohydrodynamic analysis.* Proceedings of the Institution of Mechanical Engineers, Part J: Journal of Engineering Tribology, vol. 229, iss. 4, pp. 376-397, 2015, doi: 10.1177/1350650114550346

[25] J.C. Atwal, R.K. Pandey, *Performance improvement of water-lubricated thrust pad bearing operating with the turbulent flow using a new micro-pocket design*, Tribology International, vol. 154, pp. 106738, 2020, doi: 10.1016/j.triboint.2020.106738

[26] J.C. Atwal, R.K. Pandey, *Influence of new surface micro-structures on the performance behaviours of fluid film tilting pad thrust bearings,* Proceedings of the Institution of Mechanical Engineers, Part C: Journal of Mechanical Engineering Science, vol. 236, pp. 3111-3134, 2021, doi: 10.1177/09544062211030972

[27] J.C. Atwal, R.K. Pandey, *Design of hydrodynamically lubricated a new micro-pocketed tilting pad thrust bearing based on simulated performance parameters.* Tribology in Industry, vol. 44, pp. 482-497, 2022, doi: 10.24874/ti.1286.04.22.07

[28] S. Yuan, W. Huang, X. Wang, *Orientation effects of micro-grooves on sliding surfaces,* Tribology International vol. 44, no. 9, pp. 1047-1054, 2011, doi: 10.1016/j.triboint.2011.04.007

[29] R. Rahmani, I. Mirzaee, A. Shirvani, H. Shirvani, *An analytical approach for analysis and optimisation of slider bearings with infinite width parallel textures,* Tribology International, vol. 43: pp. 1551–1565, 2010, doi: 10.1016/j.triboint.2010.02.016

[30] K.H. Huebner. *A three-dimensional thermohydrodynamic analysis of sector thrust bearing,* Transactions ASLE, vol. 7, pp. 62-73, 1974, doi: 10.1080/05698197408981439

[31] D. Vijayaraghavan, T.G. Keith, *Development and evaluation of a cavitation algorithm,* Tribology Transactions, vol. 32, pp. 225-233, 1989, doi: 10.1080/10402008908981882

[32] M. Fesanghary, M.M. Khonsari, *A modification of the switch function in the Elrod cavitation algorithm,* Journal of Tribology, vol. 133, pp. 024501-1-4. 2011, doi: 10.1115/1.4003484

[33] C.I. Papadopoulos, L. Kaiktsis, M. Fillon, *Computational fluid dynamics thermohydrodynamic analysis of three-dimensional sector-pad thrust bearings with rectangular dimples*, Journal of Tribology, vol. 136 pp. 011702-1- 11. 2014, doi: 10.1115/1.4025245

[34] J.C. Atwal, R.K. Pandey, *Film thickness and friction investigations in a fluid film thrust bearing employing a new conceived micro-texture on pads*, Journal of Tribology, vol. 143, iss. 6, pp. 061801, 2021, doi: 10.1115/1.4048500

NOMENCLATURE

β	Bulk modulus of lubricating oil, Pa
d_{pi}	Depth of pocket at inlet, m
d_{po}	Depth of pocket at exit, m
η	Lubricant viscosity, Pa-s
h	Film thickness of lubricant, m
$\bar{h}$	Non-dimensional lubricant film thickness (h/h_2)
h_1	Film thickness at inlet, m
h_2	Film thickness at exit, m
μ	Coefficient of friction
N	Speed of runner, rpm
N_r, N_θ	Number of nodes in r and θ direction
ω	Rotational speed, rad/s
p	Pressure of lubricant p, Pa
p_c	Cavitation pressure, Pa
$\bar{p}$	Normalised pressure ($ph_2^2/\eta\omega R_m^2$)
p_{cd}	Constant depth pocket
p_{vh}	Variable depth pocket (depth reduced to half along the length of pocket)
p_{vz}	Variable depth pocket (depth reduced to zero at exit)
ϕ	Fractional film content
r, θ, z	Cylindrical-coordinate in the film
$\bar{r}$	Normalized radial coordinate (r/R_m)
R_1	Pad inner radius, m
R_2	Pad outer radius, m
R_m	Mean radius, m $(R_1 + R_2)/2$
s_h	Shoulder height, m
θ	Circumferential coordinate, rad
θ_0	Sector angle of pad, degree
θ_p	Circumferential extent of pocket, degree
W	Load-carrying capacity, N
$\bar{W}$	Normalized load carrying capacity ($Wh_2^2/\eta\omega R_m^4$)